Short papers

Nonlinear Optimal Control Design for Underactuated Two-Wheeled Inverted Pendulum Mobile Platform

Sangtae Kim and SangJoo Kwon

***Abstract*—In terms of the state-dependent Riccati equation (SDRE) control framework, a nonlinear motion control is investigated for the two-wheeled inverted pendulum (TWIP) mobile robot platform. As a critical design issue, the state dependent coefficient matrix is established based on the sound understanding of dynamic characteristics of the TWIP robot. The developed SDRE control solution has the merit of robust posture stabilization when the inverted pendulum robot experiences strong nonlinear behaviors due to abrupt external disturbances.**

***Index Terms*—Personal mobility, self-balancing robot, state-dependent Riccati equation (SDRE) nonlinear control, two-wheeled inverted pendulum (TWIP).**

I. Introduction

Due to their versatility and accessibility in narrow and congested areas, two-wheeled inverted pendulum (TWIP) robots with self-balancing capability have been popularly applied as a mobile platform for personal transporters [1], [2], commuter vehicles [3], robotic wheelchairs [4], [5] as well as mobile manipulators [6], and wheeled humanoids [7]. Typically, most of the TWIP vehicles commonly follow the Segway design philosophy [1] and feature a compact-sized body and differential type steering mechanism using two parallel wheels. Because the TWIP mobile platform is an inherently unstable and nonlinear system and belongs to the underactuated system, which implements the 3-degrees of freedom (DOF) motion of pitch, yaw, and straight movement with only two actuator inputs, it has attracted great attention from the control community and recently numerous results have been reported as well-classified in [8].

As long as the TWIP maintains a small pitch angle around the equilibrium point, the self-balancing motion can be readily achieved by employing conventional linear control techniques such as PID control, pole placement, and linear quadratic regulator (LQR) [9]. However, when the TWIP robot enters into the region of nonlinear behavior with large pitch angles due to intentional maneuvers or external disturbances, the linear control methods are certainly limited in keeping the postural stability. To remedy this issue and increase the driving performance, a lot of nonlinear control approaches have been proposed, including fuzzy control [10], neuro-adaptive control [11], feedback linearization [12], and sliding control [13]. Yet, those previous works are not so appealing in that most of them are confined to suggesting the mathematical rigor and the feasibility of the nonlinear controls without providing clear experimental validations which outperform linear controllers.

To get over the performance limit of the linear controls and fully accomplish the agile motion of the TWIP robot using the self-balancing function, it is necessary to employ the dynamic characteristic into the model-based control design. To fulfill this point, a nonlinear optimal control design method is addressed in this paper in terms of the state-dependent Riccati equation (SDRE) control framework, which can be called a nonlinear system version of the LQR optimal control. It has the merit of utilizing the nonlinear system model directly in the LQR-like optimal control design, where the critical design issue lies in how to establish the state-dependent coefficient (SDC) matrix, which provides a design flexibility in the SDRE control by being engaging in determining the optimal gains.

Since it has been initiated as a classical nonlinear control approach [14], the SDRE control method has been revisited recently and shown to have theoretical possibilities for diverse nonlinear control issues as stated in the nice surveys [15]–[17]. For examples, it has been applied to the nonlinear benchmark problem [18], magnetic levitation [19], nonlinear filtering for UAV localization [20], and nonlinear control of aircraft and missiles [17]. Also, the SDRE method has been adopted in the nonlinear control of robotic systems such as flexible manipulator [21], pendubot [22], and cart-pendulum [23].

In the previous work on the SDRE control of a two-wheeled robot [24], we have remained in a preliminary study without certain design criteria for the SDC matrix. In contrast, by reflecting the dynamic characteristics of the TWIP robot into the SDC parametrization and providing experimental results, this paper is to fully argue that the SDRE control could be a promising approach for robust stabilization of the TWIP mobile platform as a nonlinear, underactuated, and multivariable system.

II. Dynamics

A. Dynamic Model of TWIP

The schematic of a TWIP robot is shown in Fig. 1 with the parameters in Table I. By applying the mathematical modeling procedure for the nonholonomic system suggested in [25] and [26], we have the nonlinear dynamic equation of motion

$$M(q)\ddot{q} + C(q,\dot{q})\dot{q} + G(q) = N\tau \tag{1}$$

where $M \in R^{3\times3}, C \in R^{3\times3}, G \in R^{3\times1}, \tau \in R^{2\times1}$ represent the inertia matrix, centrifugal and Coriolis force matrix, gravity vector, and

Manuscript received April 2, 2017; revised August 7, 2017; accepted October 24, 2017. Date of publication October 26, 2017; date of current version December 13, 2017. Recommended by Technical Editor X. Jing. This work was supported by the National Research Foundation of Korea under Grant NRF-2015R1D1A1A01061390. *(Corresponding Author: SangJoo Kwon.)*

The authors are with the School of Aerospace and Mechanical Engineering, Korea Aerospace University, Goyang 412-791, South Korea (e-mail: kimonkey@kau.ac.kr; sjkwon@kau.ac.kr).

Color versions of one or more of the figures in this paper are available online at http://ieeexplore.ieee.org.

Digital Object Identifier 10.1109/TMECH.2017.2767085

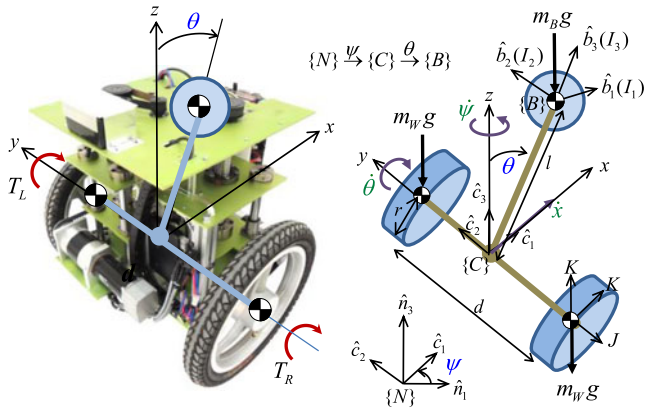

Fig. 1. Schematic of a TWIP robot prototype.

TABLE I
PARAMETERS OF TWIP ROBOT

Symbol	Definition	Specification
m_B	Mass of pendulum body	45 kg
m_W	Mass of wheel	2 kg
l	Length of pendulum	0.135 m
r	Radius of wheel	8 in
d	Distance between wheels(tread)	0.6 m
I_1, I_2, I_3	MOI of pendulum body	1.9, 2.1, 1.6 kg · m^2
K, J	MOI of wheel	0.04, 0.02 kg · m^2

input vector, respectively, and the friction terms are neglected. The generalized coordinates, $q = [x\ \theta\ \psi]^T$ include the straight movement, pitch, and yaw motion. The nonsquareness of the input matrix $N \in R^{3\times 2}$ indicates that the TWIP robot belongs to the underactuated system. The details on the elements of the matrices and vectors can be consulted in [26].

Then, by taking the inverse of the inertia matrix in (1) and defining the state vector $x = [x\ \dot{x}\ \theta\ \dot{\theta}\ \psi\ \dot{\psi}]^T$ and the input vector $u = [T_L\ \ T_R]^T$, it can be reorganized in a state-space form

$$\dot{x}(t) = f(x) + B(x)u(t) = A(x)x + B(x)u(t) \tag{2}$$

where the continuous and nonunique SDC matrix $A(\mathrm{x})$ always exists. The linear mapping through $A(\mathrm{x})$ can be called an extended linearization of the nonlinear system (1). Although there exists an infinite number of candidates for the SDC matrix, if we follow the mathematical ease used in [22]–[24] to avoid singularities by making $\sin(\theta)/\theta \to 1$ as the pitch angle goes to the zero equilibrium point, we have

$$A(x) = \begin{bmatrix} 0 & 1 & 0 & 0 & 0 & 0 \\ 0 & 0 & a_2(x) & 0 & 0 & 0 \\ 0 & 0 & 0 & 1 & 0 & 0 \\ 0 & 0 & a_4(x) & 0 & 0 & 0 \\ 0 & 0 & 0 & 0 & 0 & 1 \\ 0 & 0 & a_6(x) & 0 & 0 & 0 \end{bmatrix} \quad B(x) = \begin{bmatrix} 0 & 0 \\ b_2(x) & b_2(x) \\ 0 & 0 \\ b_4(x) & b_4(x) \\ 0 & 0 \\ b_6(x) & -b_6(x) \end{bmatrix} \tag{3}$$

where the elements are listed in Appendix A as the functions of state variables.

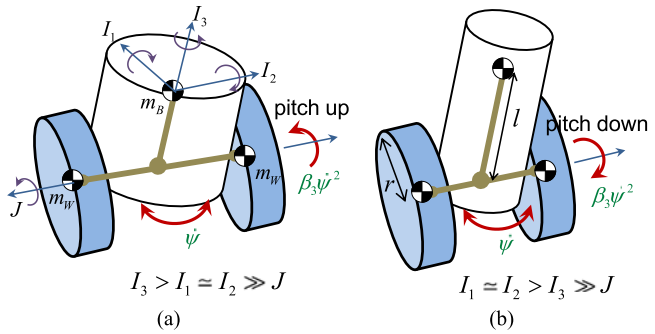

Fig. 2. Distribution of MOIs and the yaw rate effect to the pitch motion. (a) Fat body. (b) Slender body.

B. Inertial Cross Couplings

By taking the inverse of the inertia matrix in (1), the accelerations of the generalized coordinates can be expressed in the following forms:

$$\ddot{x} = \frac{1}{\eta_1(\theta)}\left(-\alpha_1 g + \alpha_2\dot{\theta}^2 + \alpha_3\dot{\psi}^2\right)\sin\theta + \alpha_4\left(T_L + T_R\right) \tag{4}$$

$$\ddot{\theta} = \frac{1}{\eta_1(\theta)}\left(\beta_1 g - \beta_2\dot{\theta}^2 - \beta_3\dot{\psi}^2\right)\sin\theta - \beta_4\left(T_L + T_R\right) \tag{5}$$

$$\ddot{\psi} = \frac{1}{\eta_2(\theta)}\left(\gamma_1\dot{\theta}\dot{\psi} - \gamma_2\dot{x}\dot{\psi}\right)\sin\theta - \gamma_3\left(T_L - T_R\right) \tag{6}$$

where $\eta_1(\theta), \eta_2(\theta)$ are given in Appendix A and the other coefficients are the functions of pitch angle or constants.

From the above equations, it can be confirmed that all the nonlinear terms get effective only when the pitch angle is deviated from the zero equilibrium point and the inertial couplings among the three axes are prevailing if the TWIP robot experiences a high yaw rate and large pitch angle simultaneously. It is also notable that the yaw motion is almost decoupled from the other axes as long as the TWIP robot maintains small pitch angles around the equilibrium point, but its effect on the other axes is relatively strong [25]. The TWIP robot undergoes that high maneuver motion when the inverted pendulum body leans forward or backward abruptly to speed up or down while driving on a circular path or turning at a spot. Actually, many rollover/turnover accidents concerned with TWIP personal transporters are happening in such situations.

The central issue in the control of a TWIP robot is to keep the inherently unstable pitch balancing motion stabilized all the time in spite of the highly nonlinear behaviors or external disturbances. Here paying our attention to the second pitch equation in (5), it consists of the gravitational force term, centripetal force terms, and the reaction torque term induced by the two wheels input, in order, where the coefficients η_1, β_1, β_2, and β_4 are always positive. It means that the centrifugal force due to the pitch rate and the reaction torque invoke a pitch-up moment to the pendulum body, while the gravity causes pitch-down motion.

However, the sign of β_3 associated with the yaw rate term could be alternating depending on the distribution of the mass moment of inertia (MOI) of the pendulum along the axes of motion as

$$\beta_3 = \left\{(I_3 - I_1)m_B + 2(I_3 - I_1 - m_B l^2)(m_W + J/r^2)\right\}\cos\theta \tag{7}$$

where the MOIs roughly satisfy the relationships denoted in Fig. 2 according to the slenderness of the pendulum body.

In the case of a fat body, it usually has a positive β_3 and the centrifugal force by the yawing motion contributes to restoring it to the zero angle by generating a pitch-up moment. The same phenomenon can be actually observed in the rotation of a top. The situation is reversed in case the robot configuration has a high slenderness and as the pendulum length gets higher. Then, it is necessary to moderate the yaw control performance because too fast steering or abrupt turning could break the pitch balancing status.

III. Nonlinear Optimal Control Design

A. SDRE Method

Given the extended linear state (2) through the SDC parametrization of the nonlinear system (1), the same design procedure as the LQR, which minimizes the infinite-time quadratic performance index

$$J(x,u)=\frac{1}{2}\int_0^\infty \left\{x^T(t)Q(x)x(t)+u^T(t)R(x)u(t)\right\}dt \qquad (8)$$

where $Q(x)\in R^{6\times 6}$ $R(x)\in R^{2\times 2}$ $Q(x)\geq 0$ $R(x)>0$ $\forall x$ leads to the suboptimal control law [15]–[17]

$$u(t)=-K(x)x(t) \text{ with } K(x)=R^{-1}(x)B^T(x)P(x) \qquad (9)$$

which makes the closed-loop system locally asymptotically stable, where $P(\mathrm{x})$ is a unique, symmetric, and positive-definite solution of the SDRE

$$P(x)A(x)+A^T(x)P(x)+Q(x) - P(x)B(x)R^{-1}(x)B^T(x)P(x)=0. \qquad (10)$$

In fact, the nonuniqueness of the SDC matrix $A(\mathrm{x})$ provides a design flexibility in the SDRE control, because it functions as a gain in addition to the weighting matrices $Q(\mathrm{x}),R(\mathrm{x})$ and enables us to adjust the performance, stability, and optimality of the closed loop system. However, it also leaves the global asymptotic stability unguaranteed, although some global stability conditions were given in [19], and how to systematically parametrize the SDC matrix still remains an unsolved open issue [17]. Hence, in order to expect a performance enhancement in terms of the SDRE nonlinear control, it is indispensable to establish the SDC matrix by resorting to the physical understanding about the TWIP dynamics.

B. LQR Versus SDRE Control

The SDC matrix given in (3) can be typically used in an inverted pendulum system since it has the advantage of preventing the singularity near zero pitch angle. In contrast, the linearization of the TWIP dynamic model around the zero equilibrium point makes the system matrix and input matrix in (3) have the constant elements in Appendix B as

$$A=\begin{bmatrix}0&1&0&0&0&0\\0&0&a_2&0&0&0\\0&0&0&1&0&0\\0&0&a_4&0&0&0\\0&0&0&0&0&1\\0&0&0&0&0&0\end{bmatrix} \quad B=\begin{bmatrix}0&0\\b_2&b_2\\0&0\\b_4&b_4\\0&0\\b_6&-b_6\end{bmatrix} \qquad (11)$$

where it should be noted that the sixth-row element of the system matrix has been removed. Then, the yaw motion is perfectly decoupled from the other axes in the linear system assumption.

The simulation results shown in Figs. 3 and 4 correspond to the two representative high maneuver behaviors where the nonlinear coupling terms of the TWIP dynamics become dominated by the large pitch angle and fast yaw rate occurring together. The results compare how the stabilizing motion of the TWIP differs when the SDRE and LQR control based on the SDC matrix in (3) and the linear system matrix in (11) are, respectively, applied to the prototype shown in Fig. 1. In Fig. 3, the robot is accelerated to move forward and the step disturbance inputs denoted in Fig. 3(c) and (d) are applied abruptly to both wheels to postulate a yaw-directional moment. Also, the same disturbance is applied in Fig. 4 when the robot is spinning at a spot with a high speed yaw rate.

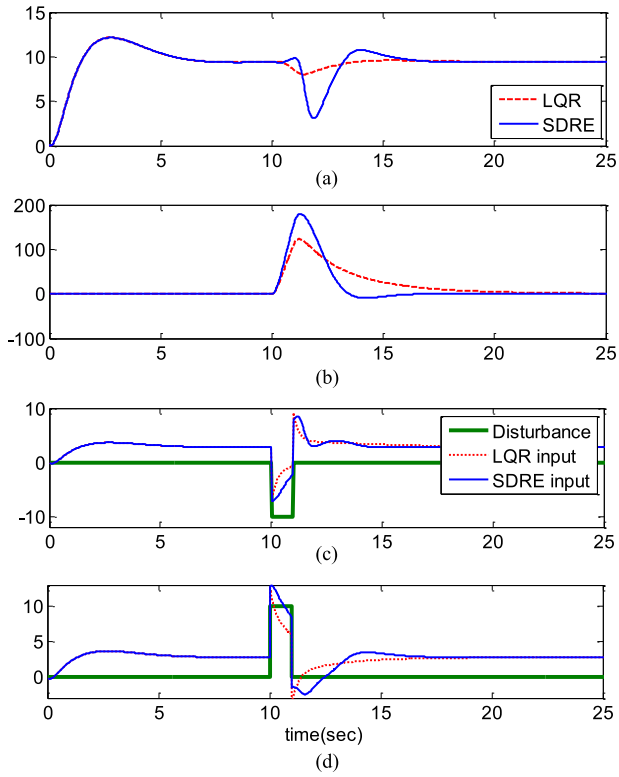

Fig. 3. Performance comparison of LQR versus SDRE control in constant forward acceleration (0.8 m/s^2). (a) Pitch angle (deg). (b) Yaw angle (deg). (c) Left wheel torque and disturbance input (Nm). (d) Right wheel torque and disturbance input (Nm).

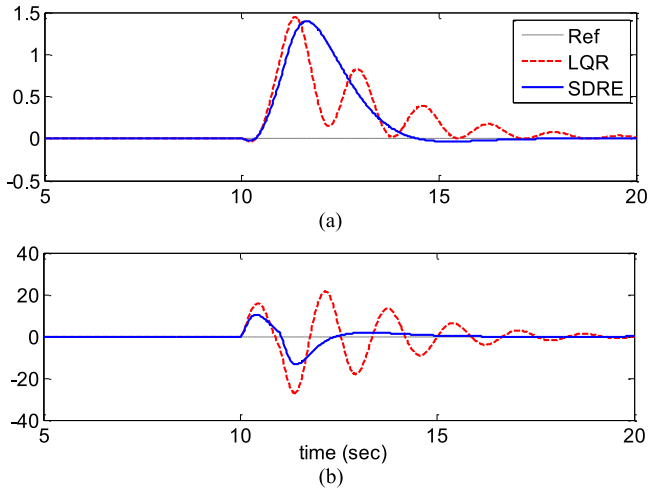

Fig. 4. LQR versus SDRE control in high-speed spinning (yaw rate 480 deg/s). (a) Straight movement (m). (b) Pitch angle (deg).

As indicated in Figs. 3 and 4, the TWIP motion is fluctuated by assigning the peak disturbance, and then, recovered to the steady state as the feedback loop is activated. The fast convergence of the state variables to the reference values and the fewer oscillations are certainly the benefits of the nonlinear control, which has been enabled because the nonlinear characteristic of the TWIP robot is reflected in determining the time-varying gain matrix in (9) through the system model in (3). However, the large overshoot that occurred in the pitch trajectory in Fig. 3 says that the SDRE control with the typical SDC matrix does not guarantee a fair pitch balancing performance all the time.

C. SDC Matrix Design

The large distortion of the pitch trajectory in Fig. 3 can be interpreted as the high gain effect of the SDC matrix involved in the SDRE (10), specifically by the sixth-row element engaged in the yaw motion control, while it is neglected in the linear system for the LQR control. As mentioned in Section II, it is true that the dynamic coupling effect of the pitch motion on the yaw-directional rotation is relatively weak, but the swift yawing action tends to severely conflict with the pitch-directional postural stability. Moreover, we have to consider the performance limit of the TWIP robot coming from the underactuated structure, that is, which implements the 3-DOF motion with only two inputs. Therefore, the yawing control performance needs to be compromised so that it does not harm the pitch balancing motion. Actually, it can be accomplished by proper parameterization of the SDC matrix as indicated in (2).

In order to keep the fairly good performance of the SDRE control demonstrated in Figs. 3 and 4, it is desirable to apply the second- and fourth-row elements the same as in the typical SDC matrix suggested in (3). However, the sixth-row elements need to be rearranged to mitigate the high gain effect, so that they show moderate changes according to the yaw rate increase and are not much affected by the magnitude of the forward velocity. As one of the possible choices, which meet these requirements, we have

$$A^*(x) = \begin{bmatrix} 0 & 1 & 0 & 0 & 0 & 0 \\ 0 & 0 & a_2^*(x) & 0 & 0 & 0 \\ 0 & 0 & 0 & 1 & 0 & 0 \\ 0 & 0 & a_4^*(x) & 0 & 0 & 0 \\ 0 & 0 & 0 & 0 & 0 & 1 \\ 0 & a_{62}^*(x) & 0 & a_{64}^*(x) & 0 & 0 \end{bmatrix} \tag{12}$$

where the elements are given by $a_2^*(x) = a_2(x)$, $a_4^*(x) = a_4(x)$, $a_{62}^*(x) = -m_P l\dot{\psi}\sin\theta/\eta_2(\theta)$, $a_{64}^*(x) = 2(I_3 - I_1 - m_P l^2)\dot{\psi}\sin\theta\cos\theta/\eta_2(\theta)$.

In a TWIP robot with the angular velocities (ω_R, ω_L) of the two wheels, the forward velocity and the yaw rate are given by

$$\dot{x} = \frac{r(\omega_R + \omega_L)}{2} \quad \dot{\psi} = \frac{r(\omega_R - \omega_L)}{d}. \tag{13}$$

For the prototype in Fig. 1, the variations of the sixth-row elements of the SDC matrices are visible in Fig. 5, where the single element in (3) makes a rapid change according to the simultaneous increase of the vehicle speed and yaw rate. In contrast, the two elements in (12), putting more emphasis on the postural stability rather than the yawing performance, maintain small values for a wide range of TWIP motion.

By applying the SDC matrices (3) and (12), respectively, to the control law in (9) with the SDRE in (10), we have the simulation result in Fig. 6 for the same situation in Fig. 3 and the same disturbance input. As a result, the SDC matrix proposed in the context of the sound understanding about the TWIP motion characteristics much improves the pitch stability at the cost of reducing the yaw convergence rate. On the other hand, for the second mission given in Fig. 4, the proposed SDC matrix produces almost the same responses as the typical one.

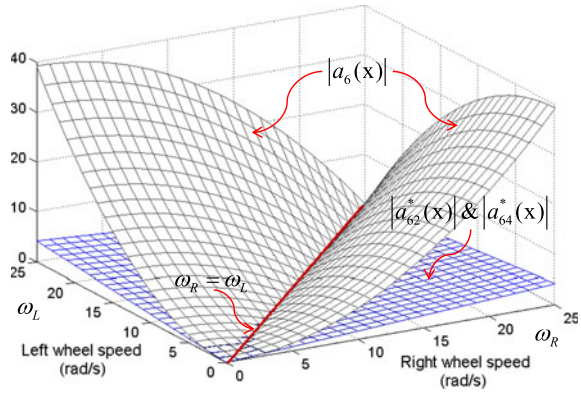

Fig. 5. Variations of the sixth-row elements of the SDC matrix according to the wheel speed (when the pitch angle is 20°).

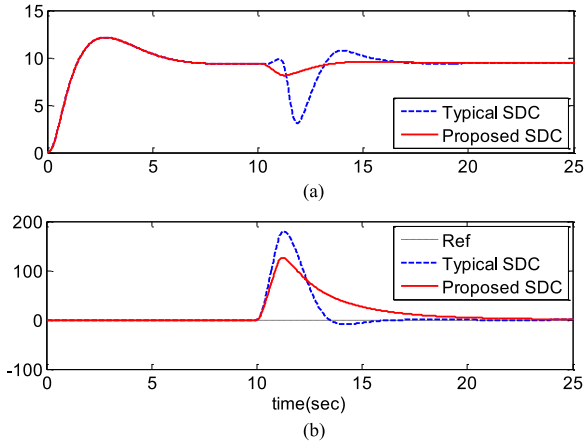

Fig. 6. Performance comparison of the two SDC matrices. (a) Pitch angle (deg). (b) Yaw angle (deg).

IV. Experiment

A. Implementation Issue

The hardware control system architecture for the prototype robot consists of two BLDC motors with encoders to estimate the forward velocity and yaw rate, attitude sensor (rate gyro) to detect the pitch rate and pitch angle, and PC with Core i5 processor to implement the optimal control law. Regarding the system bandwidth of the TWIP robot, the allowable time delay of the control loop for attitude control has been identified to be about 20 ms, while the measured delays occurring in the communication lines among the control processor and motor driver and attitude sensor are definitely below 10 ms. Hence, the timer interrupt for the control input is updated every 10 ms synchronized with the update rate of the attitude sensor.

An efficient way to solve the matrix equation SDRE in (10) is to apply the Schur decomposition [27] for the Hamiltonian matrix of the Riccati equation. The overall computation time to determine the SDRE gain matrix is at most 0.46 ms in the PC-processor on average. The control software development environment is the Microsoft Visual C++ with the LAPACK library [28]. As for the LQR control input, the same procedure is followed as in the SDRE control except that the linear system matrices in (11) with constant elements are used instead of the nonlinear system matrices in (12) where the time-varying elements are updated every control period in the SDRE control.

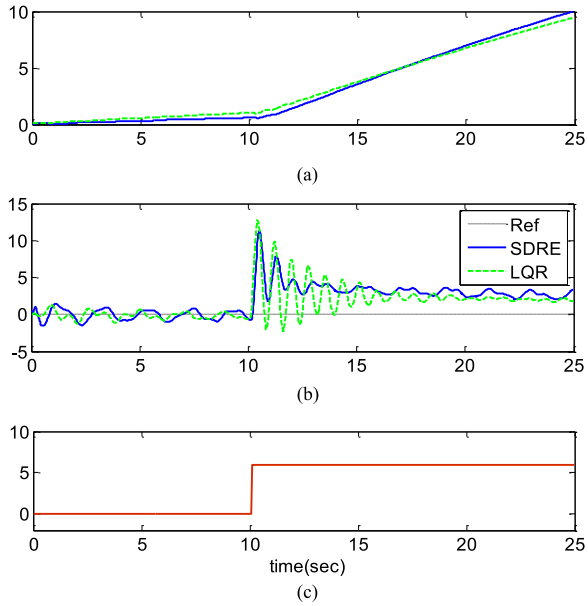

Fig. 7. Experiment of high-speed spinning with yaw rate 180 deg/s. (a) Forward movement (m). (b) Pitch angle (deg). (c) Disturbance to R/L wheels (Nm).

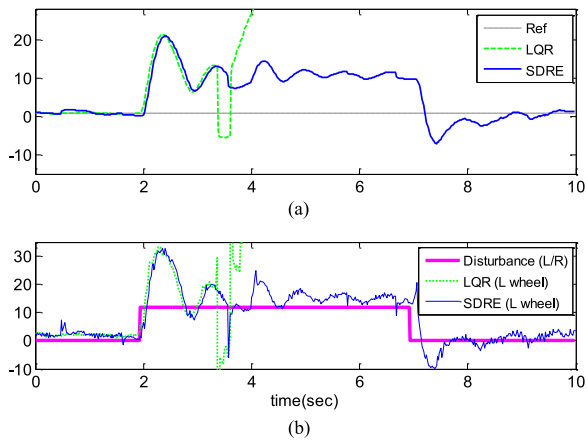

Fig. 8. Experiment of high-speed spinning with yaw rate 320 deg/s. (a) Pitch angle (deg). (b) Input (Nm).

Fig. 9. Overlapped images of the high-speed spinning. Video clips available in http://mercury.kau.ac.kr/sjkwon/publication/LQR.wmv, and SDRE.wmv.

B. Experimental Results

The effect of nonlinear control over the linear control performance will be clarified only when the TWIP robot enters into the region of strong nonlinear behaviors having large pitch angles due to the acceleration or deceleration phase and also high rates of rotational speed due to fast steering action. Although a large pitch angle can be generated when the robot is accelerated, as in the simulation result in Fig. 3, such high speed and long travel experiments require a large space and carry the risk of accident. So we consider an alternative situation as in Fig. 4 where the robot is spinning at a fixed point with a high angular velocity and a sudden disturbance is assigned to generate an arbitrary pitching moment to break the equilibrium status.

First, the robot is spinning at the rate of 180 deg/s in Fig. 7 and the disturbance torque is applied to both wheels at 10 s. Then, the pitch balancing pose is heavily peaking in the LQR control and converges to the static equilibrium against the disturbance torque while the robot is moving forward slowly. Second, when the spinning speed is raised to the higher value of 320 deg/s and the heavier disturbance torque is applied in Fig. 8, the attitude control failed in LQR and turnover happened. However, the SDRE control holds the balancing motion and finally recovers the upright posture as shown in Fig. 9. It proves the benefit of the nonlinear control enabling robust stabilization when the TWIP robot is facing heavy destabilizing moments due to external disturbances or intentional high maneuvers. The step disturbances assumed in Figs. 3, 7, and 8 cover generic situations that a TWIP robot may experience in the real world.

V. Conclusion

The TWIP balancing mobile robot platforms are being popularly applied to unmanned ground vehicles and mobile manipulators as well as commercial personal transporters. In this paper, we have presented that the SDRE nonlinear optimal control is an attractive multivariable motion control approach providing a systematic design framework for the underactuated TWIP robot. As it has been demonstrated, the SDRE control performance is guaranteed when a well-planned SDC matrix is employed. Among the two types of the proposed SDC matrices, the latter one parametrized by considering the dynamic coupling effect is preferable in the sense that it makes the pitch balancing motion more robust to the external disturbances.

Appendix

A. Elements of the Nonlinear System Matrices in (3)

$$a_2(x) = \frac{1}{\eta_1(\theta)}\left(\frac{\mathrm{s}\theta}{\theta}\right)[-m_B^2 l^2 g\mathrm{c}\theta + (I_2 + m_B l^2)m_B l\dot{\theta}^2 + m_B l\{I_2 + m_B l^2 + (I_3 - I_1 - m_B l^2)\mathrm{c}^2\theta\}\dot{\psi}^2]$$

$$a_4(x) = \frac{1}{\eta_1(\theta)}\left(\frac{\mathrm{s}\theta}{\theta}\right)\left[\left(m_B + 2M + \frac{2J}{r^2}\right)m_B l g - m_B^2 l^2\dot{\theta}^2\mathrm{c}\theta - \left(m_B^2 l^2 + (I_3 - I_1 - m_B l^2)\left(m_B + 2m_W + \frac{2J}{r^2}\right)\right)\dot{\psi}^2\mathrm{c}\theta\right]$$

$$a_6(x) = \frac{1}{\eta_2(\theta)}\left(\frac{\mathrm{s}\theta}{\theta}\right)\left(2(I_3 - I_1 - m_B l^2)\dot{\theta}\dot{\psi}\mathrm{c}\theta - m_B l\dot{x}\dot{\psi}\right)$$

$$b_2(x) = \left((I_2 + m_B l^2)/r + m_B l\mathrm{c}\theta\right)/\eta_1(\theta)$$

$$b_4(x) = -\left((m_B l\mathrm{c}\theta)/r + m_B + 2m_W + 2J/r^2\right)/\eta_1(\theta)$$

$$b_6(x) = -(d/r)/\eta_2(\theta)$$

$$\eta_1(\theta) = m_B^2 l^2\mathrm{s}^2\theta + m_B I_2 + 2(m_W + J/r^2)(I_2 + m_B l^2)$$

$$\eta_2(\theta) = I_3 + 2K + 2(m_W + J/r^2)d^2 + (I_1 + m_B l^2 - I_3)\mathrm{s}^2\theta.$$

B. Elements of the Linear System Matrices in (11)

$$a_2 = -m_B^2 g l^2/\mu_1, \quad a_4 = (m_B + 2m_W + 2J/r^2) m_B g l/\mu_1$$

$$b_2 = \left((I_2 + m_B l^2)/r + m_B l\right)/\mu_1, \quad b_6 = -(d/r)/\mu_2$$

$$b_4 = -\left((m_B l)/r + m_B + 2m_W + 2J/r^2\right)/\mu_1$$

$$\mu_1 = (m_B + 2m_W + 2J/r^2)(I_2 + m_B l^2) - m_B^2 l^2$$

$$\mu_2 = I_3 + 2K + 2(m_W + J/r^2) d^2.$$

REFERENCES

[1] How Segway Works. [Online]. Available: https://en.wikipedia.org/wiki/Segway_PT, http://youtu.be/rmlg5QkusFQ

[2] Toyota Winglet. [Online]. Available: https://en.m.wikipedia.org/wiki/Toyota_Winglet, http://youtu.be/SfwwZu1GyUc

[3] General Motors EN-V. [Online]. Available: http://en.wikipedia.org/wiki/General_Motors_EN-V, http://youtu.be/zoKxx0GEEFE

[4] H. Ustal and J. L. Minkel, "Study of the independence IBOT 3000 mobility system: An innovative power mobility device, during use in community environments," *Arch. Phys. Med. Rehabil.*, vol. 85, no. 12, pp. 2002–2010, Dec. 2004.

[5] Genny Mobility. [Online]. Available: http://www.gennymobility.com/Genny/, http://youtu.be/7DfcjRcoef0

[6] C. Acar and T. Murakami, "Multi-task control for dynamically balanced two-wheeled mobile manipulator through task-priority," in *Proc. 2011 Int. Symp. IEEE Ind. Electron.*, 2011, pp. 2195–2200.

[7] M. Stilman J. Wang, K. Teeyapan, and R. Marceau, "Optimized control strategies for wheeled humanoids and mobile manipulators," *Proc. 9th Int. Conf. IEEE-RAS Humanoid Robots*, Dec. 2009, pp. 568–573.

[8] R. P. M. Chan, K. A. Stol, and C. R. Halkyard, "Review of modeling and control of two-wheeled robots," *Annu. Rev. Control*, vol. 37, pp. 89–103, 2013.

[9] P. Oryschuk, A. Salerno, A. M. Al-Husseini, and J. Angeles, "Experimental validation of an underactuated two-wheeled mobile robot," *IEEE/ASME Trans. Mechatronics*, vol. 14, no. 2, pp. 252–257, Apr. 2009.

[10] C.-H. Huang, W.-J. Wang, and C.-H. Chiu, "Design and implementation of fuzzy control on a two-wheel inverted pendulum," *IEEE Trans. Ind. Electron.*, vol. 58, no. 7, pp. 2988–3001, Jul. 2011.

[11] Z. Li and C. Yang, "Neural-adaptive output feedback control of a class of transportation vehicles based on wheeled inverted pendulum models," *IEEE Trans. Control Syst. Technol.*, vol. 20, no. 6, pp. 1583–1591, Nov. 2012.

[12] K. Pathak, J. Franch, and S. K. Agrawal, "Velocity and position control of a wheeled inverted pendulum by partial feedback linearization," *IEEE Trans. Robot.*, vol. 21, no. 3, pp. 505–513, Jun. 2005.

[13] J.-X. Xu, Z.-Q. Guo, and T. H. Lee, "Design and implementation of integral sliding-mode control on an underactuated two-wheeled mobile robot," *IEEE Trans. Ind. Electron.*, vol. 61, no. 7, pp. 3671–3681, Jul. 2014.

[14] J. D. Pearson, "Approximation methods in optimal control," *J. Electron. Control*, vol. 13, pp. 453–469, 1962.

[15] J. R. Cloutier, "State-dependent Riccati equation techniques: An overview," in *Proc. 1997 Int. Conf. Amer. Control*, Albequerque, NM, USA, 1997, pp. 932–936.

[16] T. Cimen, "State-depedent riccati equation (SDRE) control: A survey," in *Proc. 17th World Congr. Int. Fed. Autom. Control*, Jul. 2008, pp. 3761–3775.

[17] T. Çimen, "Survey of state-dependent Riccati equation in nonlinear optimal feedback control synthesis," *J. Guid. Control Dyn.*, vol. 35, no. 4, pp. 1025–1047, Jul.–Aug. 2012.

[18] C. P. Mracek and J. R. Cloutier, "Control designs for the nonlinear benchmark problem via the state-dependent Riccati equation method," *Int. J. Robust Nonlin. Control*, vol. 8, pp. 401–433, Apr. 1998.

[19] E. Erdem and A. Alleyne, "Design of a class of nonlinear controllers via state dependent Riccati equations," *IEEE Trans. Control Syst. Technol.*, vol. 12, no. 1, pp. 133–137, Jan. 2004.

[20] A. Nemra and N. Aouf, "Robust INS/GPS sensor fusion for UAV localization using SDRE nonlinear filtering," *IEEE Sensors J.*, vol. 10, no. 4, pp. 789–798, Apr. 2010.

[21] A. Fenili and J. M. Balthazar, "The rigid-flexible nonlinear robotic manipulator: Modeling and control," *Commun. Nonlin. Sci. Numer. Simul.*, vol. 16, pp. 2332–2341, May 2011.

[22] E. Erdem and A. Alleyne, "Experimental real-time SDRE control of an underactucated robot," in *Proc. 2001 40th Int. Conf. IEEE Decis. Control*, Dec. 2001, pp. 2986–2991.

[23] P. Dang and F. L. Lewis, "Controller for swing-up and balance of single inverted pendulum using SDRE-based solution," in *Proc. 2005 31st Annu. Conf. Ind. Electron. Soc.*, Nov. 2005, pp. 304–309.

[24] S. Kim and S. J. Kwon, "SDRE based nonlinear optimal control of a two-wheeled balancing robot," *J. Inst. Control Robot. Syst.*, vol. 17, no. 10, pp. 1037–1043, Jul. 2011.

[25] S. J. Kwon, S. Kim, and J. Yu, "Tilting-type balancing mobile robot platform for enhancing lateral stability," *IEEE/ASME Trans. Mechatronics*, vol. 20, no. 3, pp. 1470–1481, Jun. 2015.

[26] S. Kim and S. J. Kwon, "Dynamic modeling of a two-wheeled inverted pendulum balancing mobile robot," *Int. J. Control Autom. Syst.*, vol. 13, no. 4, pp. 926–933, Aug. 2015.

[27] A. J. Laub, "A schur method for solving algebraic riccati equations," *IEEE Trans. Autom. Control*, vol. 24, no. 6, pp. 913–921, Dec. 1979.

[28] E. Anderson *et al.*, *LAPACK User's Guide*, 3rd ed. Philadelphia, PA, USA: SIAM, 1999.